# Ferromagnetic resonance in microwires and nanowires

L. Kraus,[1,*] G. Infante,[2] Z. Frait,[1] and M. Vázquez[2]
[1]*Institute of Physics, ASCR, CZ-18221, Praha 8, Czech Republic*
[2]*Materials Science Institute of Madrid, CSIC, E-28049 Madrid, Spain*
(Received 31 December 2010; published 24 May 2011)

Ferromagnetic resonance (FMR) in a single thin conducting ferromagnetic wire is investigated from theoretical and experimental points of view. It is shown that the wire radius, the symmetry of microwave magnetic field at the sample surface, and the skin depth (magnetic and nonmagnetic) should be considered as a whole for a correct interpretation of the microwave absorption. As a consequence, various resonance modes can be excited in metallic wires. The resonance fields of bulk samples satisfy the Kittel's resonance condition for a thin planar plate ($FMR_0$). However, as the wire radius decreases below the nonmagnetic skin depth a weak resonance peak separates from the main resonance and moves to the field fulfilling the Kittel's resonance condition for an axially magnetized cylinder ($FMR_1$). Theoretical predictions show that this "insulator" resonance mode should be the dominant one for a nanowire, where the radius is much smaller than the minimum magnetic skin depth. The existence of the two resonance modes is supported by experimental results on thin (down to 1.5-$\mu$m thick) amorphous microwires.

DOI: 10.1103/PhysRevB.83.174438 PACS number(s): 76.50.+g, 81.07.Gf

## I. INTRODUCTION

An increasing interest in microwave properties of very thin ferromagnetic wires (microwires and nanowires) has recently been noted because of their possible exploitations in novel applications.[1–7] Ferromagnetic resonance (FMR), a method well suited for the investigation of magnetic properties at microwave frequencies, has been extensively employed in the case of amorphous and nanocrystalline glass-coated microwires and nanowire arrays. However, the experimental results obtained by means of different measuring techniques for glass-coated microwires are often dissimilar and their interpretations from time to time even controversial. It should be admitted that this may be related to the fact that for many years, most FMR investigations have been performed on magnetic systems with different shapes (e.g., spheres, disks, platelets, thin films) or electrical character (i.e., nonmetallic). The diversity of interpretations specifically occurs if the skin effect in ferromagnetic metals is not properly taken into account. This fact justifies the present updating of recent progress in understanding FMR aspects of ferromagnetic metallic wires. We also predict some expectations as the wire diameter decreases to the nanoscale.

The most interesting work, though somewhat contentious, is probably the study by Lofland *et al.*[8] where FMR results on 3–6-$\mu$m-thick amorphous microwires, obtained by means of two different experimental techniques (short-ended coaxial transmission line and cavity-perturbation techniques), were compared. It was shown there that the resonance spectra obtained by the two methods are substantially different. In the case of the coaxial line technique, the maximum power absorption was observed at a magnetic field, which corresponded to an in-plane magnetized thin plate. However, in the case of cavity-perturbation technique two singularities of power absorption were observed at magnetic fields corresponding to the Kittel's resonance conditions for an axially magnetized long cylinder ($H_2$) and for an in-plane magnetized thin plate ($H_1$), respectively. At the lower field, $H_2$, a maximum of power absorption was observed, while at $H_1$ a dip in power absorption could be seen. The two singularities were ascribed to ferromagnetic resonance and antiresonance (FMAR), respectively. As will be shown later, this interpretation was far from being correct.

In the original paper by Kittel[9] it was noted that the resonance conditions derived there were only applicable if "certain dimensions of specimen are small in comparison with eddy current skin depth." Therefore special care should be taken when applying the Kittel's resonance conditions to a ferromagnetic metal. Effects of electrical conductivity and exchange interactions on FMR spectra were therefore quantitatively estimated for the first time by Kittel and Herring.[10] The FMR theory for planar in-plane magnetized metallic samples was presented by Ament and Rado[11] for bulk samples and by MacDonald[12] for plates of arbitrary thickness. In previous studies, the surface spin pinning was neglected. The general case of uniaxial surface anisotropy (either parallel or perpendicular) was initially treated by Frait and MacFaden[13] for bulk samples and by several authors for planar films of arbitrary thickness (e.g., Refs. 14 and 15). It was shown that, after corrections for the exchange-conductivity and spin pinning effects, the Kittel's resonance condition of a thin insulating planar plate can still be used even for planar metallic samples.

In the case of wire-shaped samples, however, the situation is substantially different. It was shown by Rodbell[16] that due to the skin effect the Kittel's resonance condition of a long cylinder does not apply to a thick wire. Instead of that, the resonance condition of a thin plate should be employed. If, however, the skin depth becomes comparable to or larger than the wire radius, the resonance spectrum is modified[17] depending not only on the sample dimensions but also on the particular experimental arrangement.[8,18] Ferromagnetic resonance in "mesoscopic" metallic wires (cross sections of which are comparable to skin depth) is thus interesting from both theoretical and practical points of view. In spite of this, few papers have been devoted to the theory of ferromagnetic

 

resonance in wires[17–23] and not all FMR features have been properly addressed.

The aim of this paper is therefore to review the theory of FMR in long metallic magnetic cylinders and to show how the FMR spectrum evolves when the cylinder radius decreases from the micro to the nano scale. In Sec. II the basics of FMR theory in ferromagnetic metals are outlined and the fundamental equations are introduced. The solutions for a cylinder provided by different authors are then compared in Sec. III and their advantages and drawbacks are discussed. Sec. IV is devoted to the discussion about the different resonance modes with different axial symmetries. Examples of numerical simulations of FMR spectra in wires with different diameters for a model material with the parameters typical of Fe are presented in Sec. V, while Sec. VI discusses suitable experimental arrangements for the measurements of the different FMR modes. Finally, in Sec. VII some theoretical predictions are supported by experimental results obtained on thin amorphous microwires. Theoretical and experimental results are summarized in the concluding remarks. SI units are used throughout the text, except in Secs. V and VII, where the oersted (Oe) unit is used for magnetic field, which is more suitable for experimentalists.

## II. THEORY OF FMR IN METALS

The phenomenological theory of ferromagnetic resonance in metallic materials is based on the simultaneous solution of Maxwell and Landau-Lifshitz-Gilbert equations with the appropriate boundary conditions at the air-metal interface.[11,24] In the low-level harmonic signal approximation the two linearized differential equations are obtained as (see Ref. 25)

$$\nabla^2\mathbf{h} - \operatorname{grad}\operatorname{div}\mathbf{h} = \frac{2i}{\delta_0^2}\frac{\mathbf{b}}{\mu_0}, \tag{1}$$

$$i\frac{\omega}{\gamma}\mathbf{m} = \mathbf{m}\times\left(\mathbf{H}_{\text{eff}\,0} + i\alpha\frac{\omega}{\gamma}\frac{\mathbf{M}_0}{M_s}\right) + \mathbf{M}_0\times\mathbf{h}_{\text{eff}}, \tag{2}$$

where $\mathbf{h}$, $\mathbf{m}$, $\mathbf{b}=\mu_0(\mathbf{h}+\mathbf{m})$ are the ac components of internal magnetic field, magnetization and magnetic induction, respectively. $\mathbf{M}_0$ is the dc component of magnetization, $M_s$ the saturation magnetization, $\mathbf{H}_{\text{eff}\,0}$ and $\mathbf{h}_{\text{eff}}$, are the dc and ac components of the effective field, $\omega$ is the circular frequency, $\gamma$ is the magnetomechanical ratio, $\alpha$ is the Gilbert damping constant, and $\delta_0=(2\rho/\mu_0\omega)^{1/2}$ is the nonmagnetic skin depth ($\rho$ is the resistivity of the material). The effective magnetic fields $\mathbf{H}_{\text{eff}\,0}$ and $\mathbf{h}_{\text{eff}}$ include the external magnetic field, the demagnetizing field, the effective anisotropy field, and the exchange field. In a uniformly magnetized body the dc component of exchange field is zero. This, however, does not apply to the ac component because in metals the magnetization $\mathbf{m}$ is nonuniform due to the skin effect. Then

$$\mathbf{h}_{\text{eff}} = \mathbf{h} + \mathbf{h}_{\text{anis}} + \frac{2A}{\mu_0 M_s}\nabla^2\mathbf{m}, \tag{3}$$

where $\mathbf{h}_{\text{anis}}$ is the ac component of the anisotropy field and $A$ is the exchange stiffness constant. The last term in Eq. (3) represents the exchange field and is responsible for various phenomena related to spin waves such as: the exchange-conductivity broadening of resonance line and the spin wave resonances or the surface modes.

When the exchange term is omitted ($A=0$) the solution can be substantially simplified. Then Eq. (2) represents a system of three linear equations, from which the permeability tensor can be calculated. In the Cartesian coordinate system ($x$,$y$,$z$) with the $z$ axis parallel to the dc magnetization $\mathbf{M}_0$ the permeability tensor is given by[8,26]

$$\ddot{\mu} = \begin{pmatrix} \mu_1 & -i\mu' & 0 \\ i\mu' & \mu_1 & 0 \\ 0 & 0 & \mu_0 \end{pmatrix}. \tag{4}$$

In terms of circularly polarized variables ($m_\pm = m_x \pm i\,m_y$, etc.), the permeability tensor is diagonal[26] with the following components[18]:

$$\mu_\pm = \mu_1 \mp \mu' = \mu_0\frac{H_{\text{eff}\,0} + M_s + i\alpha\omega/\gamma \pm \omega/\gamma}{H_{\text{eff}\,0} + i\alpha\omega/\gamma \pm \omega/\gamma}. \tag{5}$$

Substituting $\mathbf{b} = \ddot{\mu}\,\mathbf{h}$ into Eq. (1) and assuming solution in terms of a planar wave $\exp(iky)$ (see Ref. 11), the equation for the propagation constant $k$ is obtained:

$$k^2 = -\frac{2i}{\delta_0^2}\frac{\mu_{\text{eff}}}{\mu_0}, \tag{6}$$

where $2/\mu_{\text{eff}} = 1/\mu_- + 1/\mu_+$. The penetration depth of electromagnetic wave $\delta = 1/\text{Im}(k)$, shows the typical magnetic field dependence with the maximum at antiresonance and minimum at the resonance fields.[15] An example of skin depth calculated according to this equation for an isotropic material with parameters typical for iron ($\mu_0 M_s = 2.146$ T, $g=2.088$, $\alpha = 1.35\times10^{-3}$, $\rho = 9.7$ $\mu\Omega$m) is shown in Fig. 1. As can be seen, while the skin depth is more than 20 times larger than the nonmagnetic skin depth $\delta_0$ at ferromagnetic antiresonance, it is more than 20 times smaller at ferromagnetic resonance. This clearly indicates that just a very thin layer on the surface is involved in the ferromagnetic resonance.

When the exchange interaction is taken into account ($A \neq 0$) the term $Ak^2/\mu_0 M_s$must be added both to the nominator and denominator on the right-hand side of Eq. (5). Then Eq. (6) represents a bicubic equation for the $k$ vectors of three types of

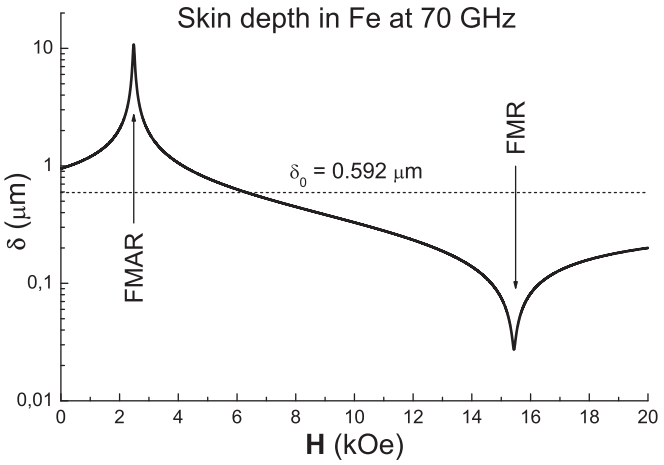


FIG. 1. Calculated magnetic skin depth $\delta$ for Fe at 70 GHz ($\mu_0 M_s = 2.146$ T, $g=2.088$, $\alpha = 1.35\times10^{-3}$, $\rho = 9.7$ $\mu\Omega$m) $\delta_0$ is the nonmagnetic skin depth. Vertical arrows denote the positions of FMR and FMAR fields.

waves (one electromagnetic and two spin waves) propagating in the ferromagnetic metal. The amplitudes of those waves can be determined from the electromagnetic and exchange boundary conditions at the air-metal interface.[24] Once these amplitudes are known the surface impedance, $\eta = e_t/h_t$, and the power absorbed by the sample,

$$P_{\text{abs}} = \int\int \text{Re}(\eta)|h_t|^2 dS, \tag{7}$$

can be calculated. $e_t$ and $h_t$ are the tangential components of microwave electric and magnetic fields, respectively, at the sample surface $S$. This equation is often used to compare the experimental results with the theory. It should be mentioned that it is suitable only for the cavity-perturbation technique, when the field $h_t$ is negligibly affected by the sample itself and can be assumed to be constant during the measurement. This assumption need not be fulfilled in FMR experiments on thin wires. Alternative formulas should be therefore used to estimate the power absorption.[18]

## III. THEORY OF FMR IN WIRES

Microwave power absorbed by a long metallic cylinder magnetized to saturation along its axis is investigated in this section. Different authors have used different approaches to solve the problem, and some of them will be briefly described here. Other orientations of external field $\mathbf{H}_0$ are discarded here because in a bulk metallic cylinder the deviation of field from the axis leads to different resonance conditions at different places of the surface and to an inhomogeneous broadening of the resonance line. Theoretical description in that case would be extremely difficult.

Let us introduce cylindrical coordinates $(r,\phi,z)$ with the $z$ axis corresponding to the axis of the cylinder (see Fig. 2). The dc field, $\mathbf{H}_0$, and the anisotropy axis of uniaxial magnetic anisotropy are supposed to lie along the $z$ axis. The general solution of Eqs. (1) and (2), nonsingular at $r=0$, can be expanded into a linear combination of cylindrical waves:

$$e^{in\phi} J_n(kr)\, e^{ik_z z}, \tag{8}$$

where $n$ is an integer number, $J_n(x)$ is the Bessel function, and $k$ and $k_z$ represent the propagation constants in the radial and axial directions, respectively. The solution can be substantially simplified if the dependence on the $z$ coordinate is neglected (i.e., $k_z = 0$). This approximation is well justified if the length of sample is small compared to the wavelength

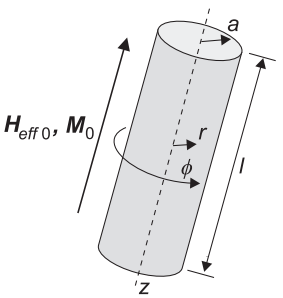


FIG. 2. Ferromagnetic wire of radius $a$ and length $l$ uniformly magnetized by an axial magnetic field $\mathbf{H}_0$. Cylindrical coordinates $(r,\phi,z)$ are shown.

of electromagnetic waves in the measuring circuit. Some authors[17,19,21,22] have also neglected the dependence on the azimuthal angle $\phi$ and considered only the axially symmetric resonance mode ($n=0$). As will be shown later, other modes can also be excited in a standard FMR experiment. Therefore, the solution for the ac magnetic field $\mathbf{h}$ inside the cylinder ($r<a$) is expected to be in the form

$$\mathbf{h}(r,\phi,z) = e^{i\omega t} \sum_n \mathbf{h}^{(n)} e^{in\phi} J_n(kr), \tag{9}$$

and similarly for magnetization, $\mathbf{m}$, magnetic induction, $\mathbf{b}$, and electric field, $\mathbf{e}$. Here $\mathbf{h}^{(n)}$ is a vectorial amplitude, depending only on frequency, $\omega$, and the dc magnetic field, $H_0$. Details of the calculation can be found in Ref. 18; only the most important points will be outlined here.

Substituting Eq. (9) into Eqs. (1) and (2) and using the orthogonality of cylindrical waves, Eq. (6) for the propagation constant, $k$, can be obtained. Solution of this equation for $A \neq 0$ provides three radial propagation constants $k_j$ ($j = U$, $S$, $N$ according to the notation by Liu and Barker[27] or $LE$, $LS$, $AS$ in Patton's notation[28]),[29] which are independent of the azimuthal mode number $n$. Thus Eq. (9) must be replaced by

$$\mathbf{h}(r,\phi,z) = e^{i\omega t} \sum_n e^{in\phi} \sum_j \mathbf{h}_j^{(n)} J_n(k_j r). \tag{10}$$

The vectorial amplitudes $\mathbf{h}_j^{(n)}$ can be determined from the air-metal boundary conditions. In order to fulfill them (continuity of $e_z$, $h_\phi$, and $b_r$ at $r=a$) the electromagnetic field outside the cylinder should be known. To do so, the wave equation for the particular measuring circuit, including the wire, must be solved. This is, however, an impractical and nearly impossible task. Different authors have consequently used different approximations to address this problem.

Lofland *et al.*[8] assume that the field outside the cylinder is the combination of a plane wave, electrically polarized along the $z$ axis, incident in the direction perpendicular to the $z$ axis and the scattered cylindrical waves propagating in the radial direction. They believe that this assumption suitably describes the situation when the wire is placed in the electric field node of a rectangular $TE_{10n}$ cavity with the microwave magnetic field perpendicular to the $z$ axis. The power absorbed by the wire is calculated using the scattering moments $A_n$ derived by Samaddar[30] for scattered plane waves by an anisotropic circular cylinder characterized by dyadic permeability and permittivity tensors. By using Eq.(33) of Ref. 30 with the permeability tensor given by Eq. (4) and the scalar relative permittivity $\varepsilon = i/(\varepsilon_0 \omega \rho)$ it can be obtained:

$$A_n = -i^n \frac{J_n(ka)}{H_n^{(2)}(ka)} \frac{\left[\frac{n}{k_1 a}\frac{k}{k_1}\frac{\mu'}{\mu_1} - \frac{k}{k_1}\frac{J_n'(k_1 a)}{J_n(k_1 a)} + \frac{1}{\varepsilon}\frac{J_n'(ka)}{J_n(ka)}\right]}{\left[\frac{n}{k_1 a}\frac{k}{k_1}\frac{\mu'}{\mu_1} - \frac{k}{k_1}\frac{J_n'(k_1 a)}{J_n(k_1 a)} + \frac{1}{\varepsilon}\frac{H_n^{(2)'}(ka)}{H_n^{(2)}(ka)}\right]}, \tag{11}$$

where $k_1 = \sqrt{\varepsilon/\mu_1}\, k \sqrt{\mu_1^2 - \mu'^2}$ and $H_n^{(2)}(x)$ is the Hankel function of the second kind. This equation can be compared with Eq. (5) of Ref. 8. Besides a different sign at the imaginary unit $i$ and $k_1$, which are unimportant, the coefficient $1/\varepsilon$ is missing in the last terms of the nominator and denominator on the right-hand side. Moreover, there is also an error in their Eq. (6). These errors probably come from an incorrect transformation of the Samaddar's equation to cgs units. In the

limit of small sample dimensions the losses can be described in terms of an effective dipole moment.[31] The power, $P$, absorbed by the unit length of the cylinder is then proportional to $\mathrm{Im}(A_{+1} + A_{-1})$.[8] This approach, however, can be used only for $n = \pm 1$. It is not applicable for the other resonance modes since their effective dipole moments are zero.

The scattering of a plane wave by an axially magnetized ferromagnetic wire has also been recently studied by Boucher and Menárd.[23] Though the paper is devoted mainly to the organized arrays of interacting nanowires, they initially investigate the response of a single wire to a locally uniform microwave magnetic field. The dipolar resonance modes, $n = \pm 1$, which are excited in this case, are described in terms of a dimension-dependent external permeability. Such an approach is more suitable to characterize properties of an individual wire in an assembly of surrounding wires. Three different levels of approximation—quasistatic (QS), extended quasistatic (EQS), and skin effect (SE)—are used to distinguish between different ranges of wire diameters.

Another method is the one used by Arias and Mills.[20] In contrast to Lofland *et al.* and Boucher and Menárd, they take into account the exchange coupling in the Landau-Lifshitz equation. Equations (1) and (2) are solved by introducing the vector potential for **e** and **h** fields. The solution for the vector potential in the same form as Eq. (9) is expected and the equations for **m** and **b** inside the cylinder are found. Outside the cylinder the microwave magnetic field is supposed to consist of the incident magnetic field $\mathbf{h}_0$, perpendicular to the $z$ axis and spatially uniform in the near vicinity of the cylinder, and the scattered field superimposing the stray fields of the modes with the azimuthal mode numbers $n = +1$ and $n = -1$, which fall off inversely with $r^2$. The unknown amplitudes of the six partial waves are found by using the electromagnetic boundary conditions and the exchange boundary conditions for the perpendicular surface anisotropy.[24] Unfortunately, further details of the calculations are missing. Instead of the absorbed power they employ the quantity

$$\Gamma = \frac{1}{h_0^2} \iint |\boldsymbol{h}|^2 \, dS \tag{12}$$

for the numerical calculations of the FMR spectra, which has little resemblance to Eq. (7).

A more general approach is used in the paper by one of the authors.[18] The electromagnetic field outside the cylinder is assumed to consist of incident and scattered cylindrical waves, which are described by formulas similar to Eq. (9) with the Bessel functions $J_n(x)$ replaced by Hankel functions $H_n^{(1)}(x)$ and $H_n^{(2)}(x)$ for the incident and scattered waves, respectively. It should be noted that any function independent of the $z$ coordinate, satisfying the wave equation, can be expanded into such series. The assumption of independence of the $z$ coordinate can be well satisfied in the vicinity of the sample, which is short compared to the electromagnetic wavelength in the measuring circuit. According to the Poynting theorem, the total power absorbed by the wire is:[18]

$$P = \sum_n P_{\mathrm{inc}}^{(n)} (1 - |A_n|^2), \tag{13}$$

where $P_{\mathrm{inc}}^{(n)}$ is the partial incident power transmitted by the cylindrical wave with the mode number $n$ and $A_n$ is the corresponding scattering moment (the ratio between the amplitudes of outward and inward waves). The scattering moments can be calculated from the boundary conditions. Thus, if the distribution of the incident power into individual cylindrical modes were known, the power absorbed by the sample could be calculated. In the following the calculations of the surface impedances $\eta_n$ and scattering moments $A_n$ are briefly outlined. The exchange coupling is initially neglected since the mathematic notation is substantially simpler and makes the text more reader friendly.

### A. Exchange neglected

As has been already mentioned, assuming $A = 0$, Eq. (6) provides only one radial propagation constant $k$ with the typical features of the "nearly uniform" ($U$) or Larmor ($LE$) electromagnetic wave. Using the notation introduced in Ref. 25, this can be labeled as the "electromagnetic approximation." Following Ref. 18 we introduce the circularly polarized variables $h_\pm$, $b_\pm$, and $m_\pm$. Then, substituting **h**, **b,** and **m** in the form of Eq. (9) into Eqs. (1) and (2) yields the following relations:

$$b_+^{(n)} = b_-^{(n)} = \mu_+ h_+^{(n)} = \mu_- h_-^{(n)} = \mu_{\mathrm{eff}} (h_+^{(n)} + h_-^{(n)})/2 = C, \tag{14}$$

for the circularly polarized components of the vectorial amplitudes $\mathbf{h}^{(n)}$ and $\mathbf{b}^{(n)}$ and Eq. (6) for $k$ vector. The circumferential magnetic field and the axial electric field of the $n$th mode inside the cylinder are then given by

$$h_\phi^{(n)}(r,\phi) = -iCe^{in\phi} \frac{1}{2} \left[ \frac{1}{\mu_+} J_{n+1}(kr) - \frac{1}{\mu_-} J_{n-1}(kr) \right], \tag{15}$$

$$e_z^{(n)}(r,\phi) = -iCe^{in\phi} \frac{\rho k}{\mu_{\mathrm{eff}}} J_n(kr), \tag{16}$$

and the surface impedance has the following expression:

$$\eta_n = \frac{e_z^{(n)}(a,\phi)}{h_\phi^{(n)}(a,\phi)} = \rho \frac{2kJ_n(ak)}{\mu_{\mathrm{eff}}[J_{n+1}(ak)/\mu_+ - J_{n-1}(ak)/\mu_-]}. \tag{17}$$

It should be mentioned that for $n = 0$ this equation is equivalent to the well known formula for the magnetoimpedance of a ferromagnetic wire.[25]

The scattering moments can be calculated imposing the electromagnetic boundary conditions (continuity of $e_z^{(n)}$ and $h_\phi^{(n)}$ at $r = a$). The boundary condition for the radial component of magnetic induction is equivalent to the boundary condition for the axial electric field. These two boundary conditions lead to two linear equations for the unknown $C$ and $A_n$. The scattering moments of the cylindrical waves are given by the formula

$$A_n = -\frac{H_n^{(1)}(a\kappa) + i\sqrt{\varepsilon_0/\mu_0}\,\eta_n H_n^{(1)'}(a\kappa)}{H_n^{(2)}(a\kappa) + i\sqrt{\varepsilon_0/\mu_0}\,\eta_n H_n^{(2)'}(a\kappa)}, \tag{18}$$

where $\kappa = \omega/c$ is the wave number in free space. By substituting for $k_1$, $\mu_1$, $\mu'$, $\varepsilon$, and using Eq. (17), the corrected

Eq. (11) by Lofland *et al.*[8] can be rewritten in a simplified form:

$$A_n = i^n \frac{J_n(a\kappa) + i\sqrt{\varepsilon_0/\mu_0}\,\eta_n J_n'(a\kappa)}{H_n^{(2)}(a\kappa) + i\sqrt{\varepsilon_0/\mu_0}\,\eta_n H_n^{(2)'}(a\kappa)}. \quad (19)$$

Equation (A13) of Ref. 23 can be also transformed into Eq. (19), with the exception of different signs at the imaginary unit, $i$, and the kind of Hankel function. This difference may come from the different frequency sign convention used in Ref. 23. The similarity between Eqs. (18) and (19) is evident. If the Bessel functions in Eq. (19) are replaced by the Hankel functions of the first kind one obtains the formula equivalent to Eq. (18). The different nominators on the right hand sides of the two equations are due to the diverse forms of the incident waves. While a plane wave is continuous everywhere, a radial wave can have a singularity at $r = 0$.

### B. Exchange included

If the exchange coupling is taken into account three waves ($U$, $S$, $N$), characterized by the azimuthal number $n$ exist for each resonance mode. Then there are two additional unknown parameters, namely the amplitudes of waves $S$ and $N$, which should be determined. The exchange boundary conditions[24] provide two additional equations for the calculation of these amplitudes. Using the general Rado and Weertman boundary condition we obtain:

$$\mathbf{M} \times \left( \frac{\partial \mathbf{M}}{\partial \mathbf{n}} - \frac{M_s^2}{2A} \frac{\partial E_{\text{surf}}}{\partial \mathbf{M}} \right) = 0, \quad (20)$$

where $\mathbf{n}$ is the normal vector of the surface and $E_{\text{surf}}$ is the surface anisotropy energy, for the cylindrical surface.[32] With uniaxial anisotropy one gets the linearized ($|\mathbf{m}| \ll |\mathbf{M}_0|$) boundary condition:

$$\mathbf{M}_0 \times \left[ \frac{\partial \mathbf{m}}{\partial r} - \frac{K_s}{A} (\mathbf{m} \cdot \mathbf{n}_a) \mathbf{n}_a \right] - \frac{K_s}{A} (\mathbf{M}_0 \cdot \mathbf{n}_a) \mathbf{m} \times \mathbf{n}_a = 0, \quad (21)$$

where $K_s$ is the surface anisotropy constant and $\mathbf{n}_a$ is the unit vector parallel to the anisotropy axis. While parallel surface anisotropy ($\mathbf{n}_a \parallel z$) was the only one considered in the previous paper[18], here a more general case is taken into account—when $\mathbf{n}_a$ is parallel to any of the cylindrical axes. Then it can be written that

$$\left[ \frac{\partial m_r}{\partial r} - p m_r \right]_{r=a} = 0, \quad \left[ \frac{\partial m_\phi}{\partial r} - q m_\phi \right]_{r=a} = 0, \quad (22)$$

where $p = q = -K_s/A$ for $\mathbf{n}_a \parallel z$, $p = K_s/A$, $q = 0$ for $\mathbf{n}_a \parallel r$, and $p = 0$, $q = K_s/A$ for $\mathbf{n}_a \parallel \phi$.

Following the procedure described in Ref. 18, the surface impedance of $n$th resonance mode is obtained from the formula

$$\frac{\eta_n}{\rho} = -\frac{\begin{vmatrix} W_{n,U}(a) & W_{n,S}(a) & W_{n,N}(a) \\ X_{n,U}(a,p) & X_{n,S}(a,p) & X_{n,N}(a,p) \\ Y_{n,U}(a,q) & Y_{n,S}(a,q) & Y_{n,N}(a,q) \end{vmatrix}}{\begin{vmatrix} V_{n,U}(a) & V_{n,S}(a) & V_{n,N}(a) \\ X_{n,U}(a,p) & X_{n,S}(a,p) & X_{n,N}(a,p) \\ Y_{n,U}(a,q) & Y_{n,S}(a,q) & Y_{n,N}(a,q) \end{vmatrix}}, \quad (23)$$

where $V$, $W$, $X$, and $Y$ are functions defined as

$$\begin{aligned} V_{n,j}(r) &= \frac{1}{2}\left[ \frac{1}{\mu_{-,j}} J_{n-1}(k_j r) - \frac{1}{\mu_{+,j}} J_{n+1}(k_j r) \right] \\ W_{n,j}(r) &= \frac{k_j}{\mu_{\text{eff,j}}} J_n(k_j r) \\ X_{n,j}(r,\xi) &= \left( \frac{1}{\mu_0} - \frac{1}{\mu_{-,j}} \right) [k_j J_{n-1}'(k_j r) - \xi J_{n-1}(k_j r)] \\ &\quad + \left( \frac{1}{\mu_0} - \frac{1}{\mu_{+,j}} \right) [k_j J_{n+1}'(k_j r) - \xi J_{n+1}(k_j r)] \\ Y_{n,j}(r,\xi) &= \left( \frac{1}{\mu_0} - \frac{1}{\mu_{-,j}} \right) [k_j J_{n-1}'(k_j r) - \xi J_{n-1}(k_j r)] \\ &\quad - \left( \frac{1}{\mu_0} - \frac{1}{\mu_{+,j}} \right) [k_j J_{n+1}'(k_j r) - \xi J_{n+1}(k_j r)] \end{aligned} \quad (24)$$

Equation (23) for the surface impedance $\eta_n$ is much more complicated because all three waves, $U$, $S$, and $N$, now take part in the calculations. The exchange coupling, however, has no effect on the electromagnetic boundary conditions, so the formulas for the scattering moments, derived in Sec. III A can still be used.

## IV. DISCUSSION

It has been shown that the magnetization $\mathbf{m}$ in a wire irradiated by microwaves consists of many oscillatory modes with different azimuthal numbers $n$. The amplitude of the individual modes depends on the spatial distribution of incident electromagnetic field in the vicinity of the sample. Consequently, the resonance curves depend on the particular experimental arrangement, as has been previously observed,[8,18] and the modes with the same axial symmetry as the incident magnetic field are most intensively excited. Since the microwave magnetic field does not have multipolar symmetry in the usual experimental conditions, the modes with azimuthal numbers $n = 0, \pm 1$ are the predominant ones. The distributions of magnetization $\mathbf{m}$ for modes $n = 0$ ("circumferential mode") and $n = 1$ ("dipolar mode") are schematically depicted in Fig. 3. Because of the axial symmetry of the $n = 0$ mode the average coupling $\langle \mathbf{m} \cdot \mathbf{h} \rangle$ of this mode with a uniform microwave magnetic field, $\mathbf{h}$, is zero.

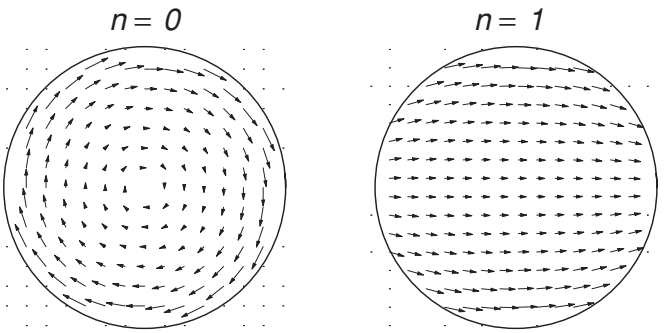


FIG. 3. Distributions of magnetization $\mathbf{m}$ inside the wire for resonance modes $n = 0$ ("circumferential mode") and $n = 1$ ("dipolar mode").

On the other hand, the dipolar magnetic moment of $n=1$ mode is responsible for a large coupling with such field. In coaxial-line-like FMR arrangements, where the circumferential microwave field is induced by a current passing through the wire, the circumferential mode, $n=0$, is mainly induced. If, however, the sample is placed in a nearly uniform transversal microwave magnetic field and zero axial electric field, the mode $n=1$ is preferentially excited (the mode $n=-1$ corresponds to the anti-Larmor precessional motion of magnetization).

The power absorbed per unit length of wire by an individual mode can be calculated either from a modified Eq. (7),

$$P_n = \mathrm{Re}(\eta_n) a \int_0^{2\pi} \left| h_\phi^{(n)}(a,\phi) \right|^2 d\phi, \tag{25}$$

if the amplitude of the corresponding circumferential magnetic field $h_\phi^{(n)}$ on the surface is known, or from

$$\frac{P_n}{P_{\mathrm{inc}}^{(n)}} = 1 - |A_n|^2 = \mathrm{Re}(\eta_n) \times \frac{8\sqrt{\varepsilon_0/\mu_0}}{\pi a\kappa \left| H_n^{(2)}(a\kappa) + i\sqrt{\varepsilon_0\mu_0}\,\eta_n H_n^{(2)'}(a\kappa) \right|^2}, \tag{26}$$

if the power $P_{\mathrm{inc}}^{(n)}$ of the incident cylindrical wave is known. Comparing these two last equations, it is deduced that the last term in Eq. (26) is proportional to the average of the square of the circumferential magnetic field on the surface. As will be shown later, not only the field (or frequency) dependence of the surface impedance $\eta_n$ exhibits the resonance behavior. It can also be $h_\phi^{(n)}$ that is responsible for resonance.

Using the asymptotic formulas for cylindrical waves, it has been shown in Ref. 18 that for large wire radius $a$ (larger than the maximum penetration depth) the surface impedances, $\eta_n$, of all modes are equal to the surface impedance of a planar half-space.[11] Then, the resonance fields of all modes are identical and equal to the Kittel's resonance field for a planar plate:

$$\omega/\gamma = \sqrt{H_{\mathrm{eff}\,0}(H_{\mathrm{eff}\,0} + M_s)}. \tag{27}$$

On the other hand, for wire radius $a$ much smaller than the minimum penetration depth, the resonance fields of different modes are different. While the resonance field of the circumferential mode can be described by Eq. (27) the resonance field of the dipolar mode satisfies the Kittel's resonance condition for the uniform precession mode of an axially magnetized infinite cylinder, i.e.:

$$\omega/\gamma = H_{\mathrm{eff}\,0} + M_s/2. \tag{28}$$

At this field the surface impedance $\eta_1$ does not show any resonance or strong frequency dependence. As Arrias and Mills[20] pointed out, the power absorption at this resonance is caused by an increase of the dipolar field around the cylinder, i.e., by $h_\varphi^{(1)}$ in Eq. (25). This means that the resonance modes $n=0$ and $n=1$ are substantially different in nature and can be also called "metallic" and "insulator" modes, respectively.

So far the limiting cases of large and small radius of the cylinder have been discussed, concluding that Eqs. (27) and (28) are the possible resonance conditions for a metallic wire. They are, however, sometimes misinterpreted in literature as they are valid under completely different experimental circumstances. In the following section some numerical simulations of resonance curves will be shown and the transition from large to small wire radius will be discussed in further detail.

## V. NUMERICAL CALCULATIONS

The numerical calculations of surface impedance $\eta_n$ according to Eq. (23) and the scattering moduli $A_n$ according to Eq. (18) have been done using Mathematica®. The program was initially tested by comparing our results with some calculations made by other authors. In spite of the errors found in the paper by Lofland *et al.*[8] and a somewhat different approach used by Arrias and Mills,[20] our calculations agree qualitatively well with their results. Parameters typical for iron are used in this section: $\mu_0 M_s = 2.146$ T, $g=2.088$, $\alpha = 1.35\times10^{-3}$, $\rho = 9.7$ $\mu\Omega$m, and $A = 2\times10^{-11}$ J/m. For the sake of simplicity the magnetocrystalline anisotropy is neglected. The surface anisotropy is omitted ($K_s=0$), unless otherwise indicated. A microwave frequency of 70 GHz is selected, which is high enough for the observation of ferromagnetic antiresonance in Fe.

### A. Circumferential (metallic) mode ($n=0$)

The dependence of $\eta_0$ and $A_0$ on dc magnetic field $H$ were calculated for several wire diameters $d=2a$ decreasing from 100 $\mu$m [well above the maximum penetration depth at FMAR (see Fig. 1)] to 50 nm (less than the minimum penetration depth at FMR). For the largest diameter $\mathrm{Re}(\eta_0)$ and $P_0$ curves are identical, showing the typical minimum close to the antiresonance field $H_a = \omega/\gamma - \mu_0 M_s = 2.480$ kOe ($1.973\times10^5$ A/m) and the maximum close to the resonance field $H_{r0} = 15.434$ kOe ($1.228\times10^6$ A/m) given by Eq. (27). As the wire diameter decreases, the antiresonance minimum broadens and finally disappears for $a<1$ $\mu$m,[18] i.e., well before the radius reached the nonmagnetic skin depth $\delta_0$. The $P_0$ curves near the resonance field are shown in Fig. 4 for different values of $a$. With decreasing diameter the resonance

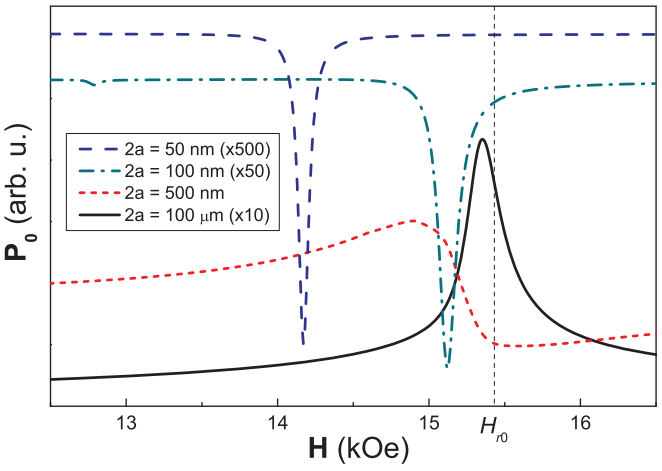


FIG. 4. (Color online) Calculated microwave power absorbed by the circumferential mode, $n=0$, for different values of the wire radius $a$. Vertical dashed line denotes resonance field calculated according to Eq. (27).

curve first becomes asymmetric and then the absorption maximum changes to minimum. The most significant changes are observed when the wire diameter is around $\delta_0$. For the real part of the surface impedance $\eta_0$, only changes of symmetry can be observed around $d \approx \delta_0$ but the character of the curve does not change. This behavior must be therefore attributed to a huge drop of the circumferential field $h_\phi^{(0)}$ at the resonance.

On the other hand, when the wire radius decreases to the minimum skin depth of the electromagnetic wave $U$ (27.4 nm) and beyond, the resonance line becomes narrower and shifts to lower fields.[17,18] That shift is proportional to $A/a^2$, which indicates that this phenomenon is caused by the exchange coupling. It has been proposed that when the microwave field penetrates to the axis of the cylinder the vortexlike structure of magnetization $\mathbf{m}^{(0)}$ around the axis (see Fig. 3) increases the exchange energy and causes the shift of the resonance field.[18] The narrowing of the resonance curve is caused by the reduction of the exchange-conductivity broadening so that the linewidth approaches the natural linewidth given by the Landau-Lifshitz-Gilbert damping.

The small dip at 12.8 kOe observed in Fig. 4 on the resonance curve for $2a = 100$ nm is caused by the radial-spin-wave resonance (SWR).[18] Similarly to the case of thin films, additional resonance peaks are observed below the main resonance, which correspond to standing spin waves with different numbers of nodes in the radial direction. The influence of the parallel surface anisotropy ($\mathbf{n}_a \parallel z$) on the spin wave resonance spectra is shown in Fig. 5. As can be seen, the spin waves are weakly excited for $K_s = 0$ and become more intense as the magnitude of surface anisotropy increases. For positive $K_s$ (easy direction along the wire axis) the SWR excitation is more effective. The surface anisotropy causes not only the increase of SWR intensity but also a shift in the SWR spectra. For example, positive $K_s$ shifts the spectrum downwards, i.e., in the same sense as the bulk anisotropy. Radial-spin-wave resonances have already been observed in a very thin amorphous FeCoPB microwire with a diameter of 2 $\mu$m.[33]

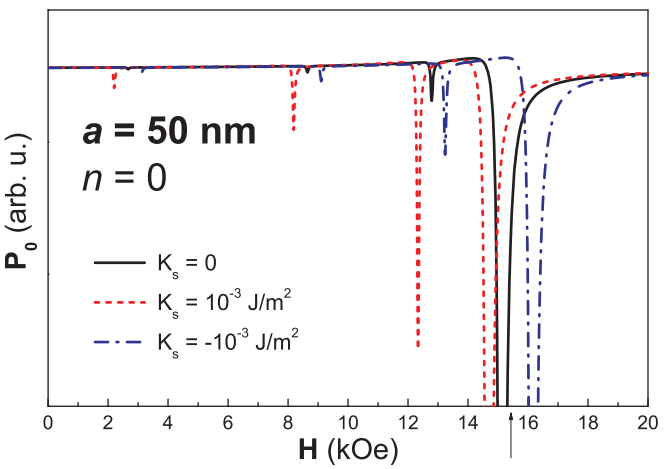


FIG. 5. (Color online) Influence of parallel surface anisotropy $K_s$ on the spin wave resonance spectra of $n = 0$ mode. Arrow denotes the resonance field calculated according to Eq. (27).

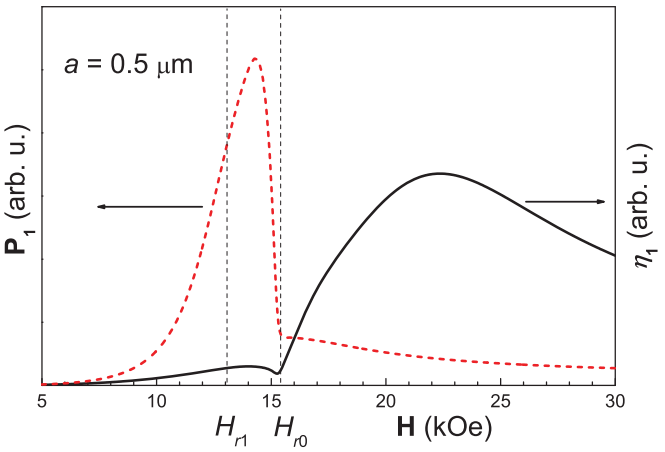


FIG. 6. (Color online) Surface impedance $\eta_1$ and absorbed microwave power $P_1$ for the "insulator mode" $n = 1$. Wire radius is $a = 0.5$ $\mu$m. Vertical dashed lines denote calculated resonance fields for $n = 1$ and $n = 0$ modes.

### B. Dipolar (insulator) mode ($n = 1$)

It was shown in previous sections that for large wire diameters the surface impedance of the dipolar mode $\eta_1$ is identical to $\eta_0$. The same applies to the power absorption $P_1$ and $P_0$. As in the case of circumferential mode, the antiresonance behavior gradually disappears when the wire radius decreases to the nonmagnetic skin depth $\delta_0$. With decreasing radius, however, $P_1$ and $\eta_1$ curves behave in a completely different way: While the maximum of $P_1$ moves to lower fields, the maximum of $\eta_1$ shifts in the opposite direction. This is demonstrated in Fig. 6, where the two curves for $a = 0.5$ $\mu$m (close to the nonmagnetic skin depth $\delta_0 = 0.592$ $\mu$m) are shown. Both curves display a small dip at the resonance field $H_{r0}$ and broad peaks on the opposite sides. The $P_1$ curve resembles the resonance curves measured by the cavity-perturbation method and calculated by Lofland *et al.*[8] The dissimilarity of $P_1$ and $\eta_1$ indicates that in wires with diameters comparable or smaller than the nonmagnetic skin depth the power absorption at FMR is not caused by the surface impedance but by the stray field of magnetic charges induced by magnetization precession.[20] Thus, for small wire diameters the surface impedance $\eta_1$ loses its meaning.

The absorption curves calculated for different values of $a$ are shown in Fig. 7. As the wire radius decreases, the resonance peak becomes asymmetric, broadens, and its maximum shifts towards the resonance field $H_{r1} = 13.153$ kOe ($1.047 \times 10^6$ A/m) corresponding to Eq. (28). For wire radius below the nonmagnetic skin depth, the resonance field does not move anymore and only the linewidth decreases,[23] similarly to the case of $n = 0$.

The standing spin wave resonances can also be excited in case of $n = 1$ mode. The SWR spectra calculated for different magnitudes of parallel surface anisotropy are shown in Fig. 8. Substantial differences in the resonance spectra are observed between the two resonance modes. First, no spin wave resonances are observed for free surface spins ($K_s = 0$), in contrast to $n = 0$. Second, the distances between the resonance fields are smaller. Third, the intensity of spin waves falls more rapidly with increasing SWR mode number. Fourth, satellites

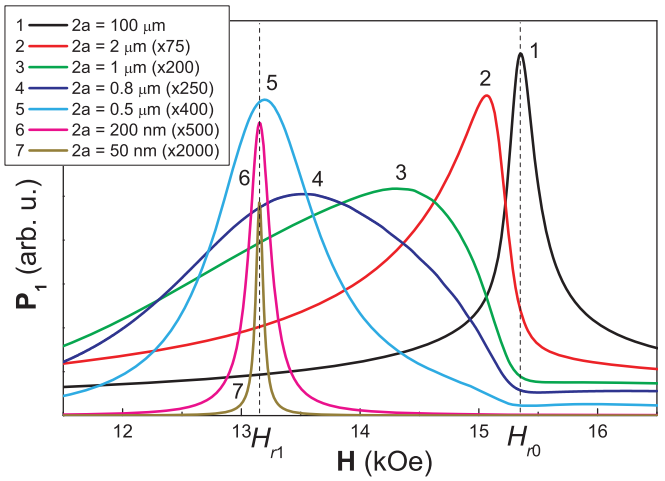


FIG. 7. (Color online) Microwave power absorbed by the "insulator mode" $n = 1$ for different values of wire radius $a$.

can be even observed above the main resonance peak. As in the case of $n = 0$, surface anisotropy shifts the SWR spectra. A more detailed discussion of spin wave resonance in very thin cylindrical wires will be published elsewhere.

## VI. FMR EXPERIMENTAL ARRANGEMENTS

Ferromagnetic resonance experiments in wires can be basically divided into two categories. They are either measurements at a fixed dc magnetic field varying the microwave frequency or measurements at a constant frequency varying the dc magnetic field. The former are done by means of network analyzers and coaxial or microstrip microwave circuits. The latter make use of classical FMR spectrometers and waveguide microwave techniques.

The coaxial line technique was originally proposed by Johnson and Rado[34] for bulk cylindrical samples and modified by Ménard *et al.*[35] for thin wires. The sample, which plays the role of the central conductor of a short-ended coaxial line, is excited by the high-frequency circumferential magnetic field

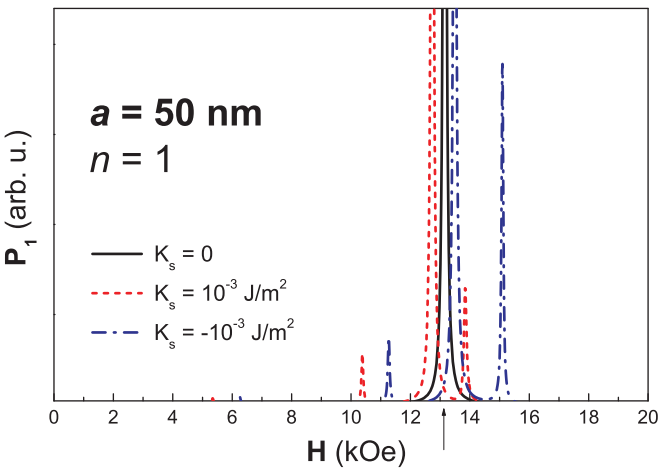


FIG. 8. (Color online) Influence of parallel surface anisotropy $K_s$ on the spin wave resonance spectra of absorption mode $n = 1$. Arrow denotes resonance field calculated according to Eq. (28).

induced by a microwave current passing through the wire. Under these conditions only the circumferential mode ($n = 0$) can be excited. Other alternatives using a network analyzer for FMR measurements in wires have been proposed: the TEM transmission line technique,[36] the microstrip line,[37] and the coaxial line short-ended by the wire[38] also use the microwave current passing through the sample. In all those arrangements the microwave field, **h,** around the sample needs not be exactly axially symmetric, so that the higher-order modes can, in principle, also be excited. Nevertheless, the field is produced mainly by the axial current so that the circumferential mode is much more intense and masks the $n = 1$ mode. A completely different approach is the method introduced by García-Miquel *et al.*[39]: A set of wires replaces the dielectric between the inner and outer conductors of the coaxial line. The wires are said to lie parallel along the axis of the coaxial line. In this case, there should be no axial current induced in the samples. The $n = 1$ mode should be excited by using this method since the external magnetic field, $\mathbf{h}_0$, of TEM wave propagating in an unperturbed coaxial line is perpendicular to the wire axis and nearly uniform in the wire volume. If, however, there is some misalignment of the wires, the axial component, $e_z$, of the electric field does not completely vanish. As is explained in the following paragraphs, this may lead to the electric polarization of the wires and to the predominant excitation of the mode would be again $n = 0$. This is evidently the case of the experimental results described in the paper by Lofland *el al.*[8]

Though many FMR experiments on glass-covered microwires have been done using network analyzers, the most common and old technique is the classical FMR spectrometer. In this case the wire is usually placed in a rectangular or cylindrical cavity or waveguide. Commercial electron paramagnetic resonance (EPR) spectrometers, which are frequently used for such measurements, are commonly equipped with rectangular or cylindrical $TE_{102}$ cavities and the specimen placed in the center, where the microwave magnetic field is maximum and nearly homogeneous. The power absorbed by the specimen is detected as a small change of the quality factor of the cavity (cavity-perturbation method). This experimental arrangement is particularly well suited for paramagnets, small insulating ferromagnets, as well as for thin metallic films. Nevertheless, it is less suitable for bulk ferromagnetic metals because even a small displacement of the sample from the node of electric field leads to the polarization of the sample which will produce large eddy currents. These currents can cause a huge drop of the quality factor and moreover a shift of the cavity resonance frequency, which undesirably affect the measurements. For this reason self-made equipment, where a part of waveguide or cavity wall is replaced by the sample surface, should be used for more precise FMR measurements on bulk ferromagnetic metals.

On the other hand, the electric polarization of an elongated metallic sample, such as a wire, if properly used, can be employed for a substantial improvement of sensitivity of such measurements. This effect was already investigated by Rodbell in 1959.[16,40] He showed that if the sample is placed in the cavity (or waveguide) with its long axis parallel to the electric field, $\mathbf{e}_0$, of the unperturbed cavity, then it is periodically polarized by longitudinal electric currents, which

are proportional to the electric field strength. These currents produce a strong circumferential magnetic field, $h_\phi$, which can be several orders higher than the maximum magnetic field, $\mathbf{h}_0$, of the unperturbed cavity. Using a simple point-charge model, Rodbell estimated that the field $h_\phi$ should be proportional to $l^2$, where $l$ is the sample length. Then the power, $P$, absorbed by the sample is proportional to the fifth power of $l$ (Ref. 40). This effect can be used for the "amplification" of FMR signal in tiny samples and was applied for investigating the nonlinear FMR behavior of ferromagnetic metals,[41] which otherwise would require very high intensities of microwave magnetic field.

It is evident that the above described polarization effect in wires produces a large circumferential magnetic field, $h_\phi^{(0)}$, which is responsible for the excitation of the circumferential ($n=0$) mode with the resonance field given by Eq. (27). The polarization effect can be rather strong even if a small component of electric field, $\mathbf{e}_0$, is parallel to the wire axis. That is why in the vast majority of FMR experiments on glass-covered microwires only the $n=0$ mode has been observed. This is probably also the case of the experimental arrangements by Garcia-Miquel *et al.*,[39] previously discussed. In order to be able to observe the $n=1$ mode it is important to take special care of the experimental arrangement to eliminate the electric polarization of the sample in the microwave cavity.[8] A simple way to observe both resonance modes simultaneously is to insert the wire sample in the middle of a rectangular $TE_{10}$ waveguide with its axis parallel to the shorter side and to short-end the waveguide by a tuning plunger (see, e.g., Ref. 33). The microwave field distributions in an unperturbed waveguide are schematically shown in Fig. 9. The transversal components of the electric, $e_{0z}$, and magnetic, $h_{0y}$, fields are proportional to $\sin(2\pi x/\lambda_g)$ and $\cos(2\pi x/\lambda_g)$, respectively, where $x$ is the distance from the tuning plunger and $\lambda_g$ the electromagnetic wavelength in the waveguide. If we neglect the higher-order resonance modes, which are only very weakly excited, the power absorbed by the wire can be roughly described by the following equation:

$$P/P_{\rm inc} = C_e l^5 \mathrm{Re}(\eta_0)\sin^2(2\pi x/\lambda_g) + C_h l \mathrm{Re}(\eta_1)\cos^2(2\pi x/\lambda_g), \qquad (29)$$

where $C_e$ and $C_h$ are constants. It can be seen that, by changing the position of tuning plunger $x$, the relative intensities of the circumferential ($n=0$) and dipolar ($n=1$) modes can be modified. Because the first term on the right-hand side is usually several orders of magnitude larger than the second one, the plunger must be precisely tuned to the position $x = (2m+1)\lambda_g/4$, where $e_0 z = 0$, in order to be able to observe the $n=1$ mode. This is the base of the method employed for the measurements described in the following section.

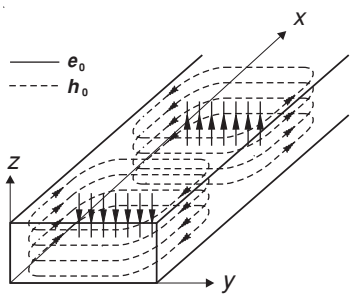


FIG. 9. Microwave field distributions in an unperturbed rectangular waveguide.

## VII. EXPERIMENTAL

In order to sustain the theoretical results described above, classical FMR experiments were done on thin, amorphous glass-covered microwires with nominal composition $Fe_{76}Si_9B_{10}P_5$ produced by the Taylor-Ulitovsky method.[42,43] Wires with two different metallic core diameters, $2a = 27$ and 1.5 $\mu$m, and total diameters 49 and 28 $\mu$m, respectively, were investigated. These two samples were selected because the first one represents a bulk sample, from a FMR point of view, while the second is among the thinnest available at the moment. Measurements were done at microwave frequencies of 49.1 and 69.7 GHz. The nonmagnetic skin depths $\delta_0$ at those frequencies are 2.4 and 2.0 $\mu$m, respectively (considering $\rho = 1.1$ $\mu\Omega$m). The radius of the thicker sample is much larger than $\delta_0$, while the second one is comparable to the skin depth. Pieces ~1.2 mm long were cut from the wires, inserted into quartz capillaries and placed into the middle of a 4-mm circular $TE_{10}$-mode waveguide with the sample axis along the electric field vector. The waveguide was finally short-ended by a plunger allowing very fine tuning of its position. In order to find the node of magnetic field in the waveguide a dummy sample of DPPH (diphenylpicrylhydrazyl) was used. The standard field modulation technique (modulation fields up to 3 Oe at 95 kHz) was employed to obtain the field derivative, $dP/dH$, of the absorbed power.

The FMR spectra measured on the 27-$\mu$m-thick sample in a position close to the maximum of electric field ("Rodbell position") are shown in Fig. 10. Both ferromagnetic resonance and ferromagnetic antiresonance peaks can be clearly observed. The Kittel resonance fields of $n=0$ mode $H_a = \omega/\gamma - M_s$ and $H_{r0}$, calculated according to Eq. (27), denoted by vertical dashed lines in the figure, well agree with the measured ones for the parameters $g = 2.09$, $\mu_0 M_s = 1.422$ T, and anisotropy field $H_K = 0$. The field derivative of the real part of surface impedance $d\mathrm{Re}(\eta_0)/dH$, calculated according to Eq. (23) with the same $g$, $M_s$, and $H_K$ and the rest of the parameters, $\alpha = 4.2\times10^{-3}$, $A = 5\times10^{-12}$ J/m, and $K_s = 0$, are shown by the dashed lines. For such thick wire, the curves practically coincide with the curves $dP_0/dH$ calculated from Eq. (26). As can be seen, the antiresonance curves are symmetric, while the experimental derivative FMR curves are rather distorted. This occurs most probably because the sample represents a large load to the microwave circuit, so that in the resonance region the reflected signal, measured by the detector, is not purely determined by the sample absorption, but also by the dispersion component.[18] This is also in the origin of the difference between the resonance fields of the measured and calculated FMR curves. When the plunger is set so that the sample is as close as possible to the node of the electric field, the intensity of the FMR peak becomes more than two orders smaller and no additional peaks can be observed. Besides that, it is impossible to distinguish between the $n=0$ and $n=1$ modes as these peaks merge for large wire diameters according to the theory.

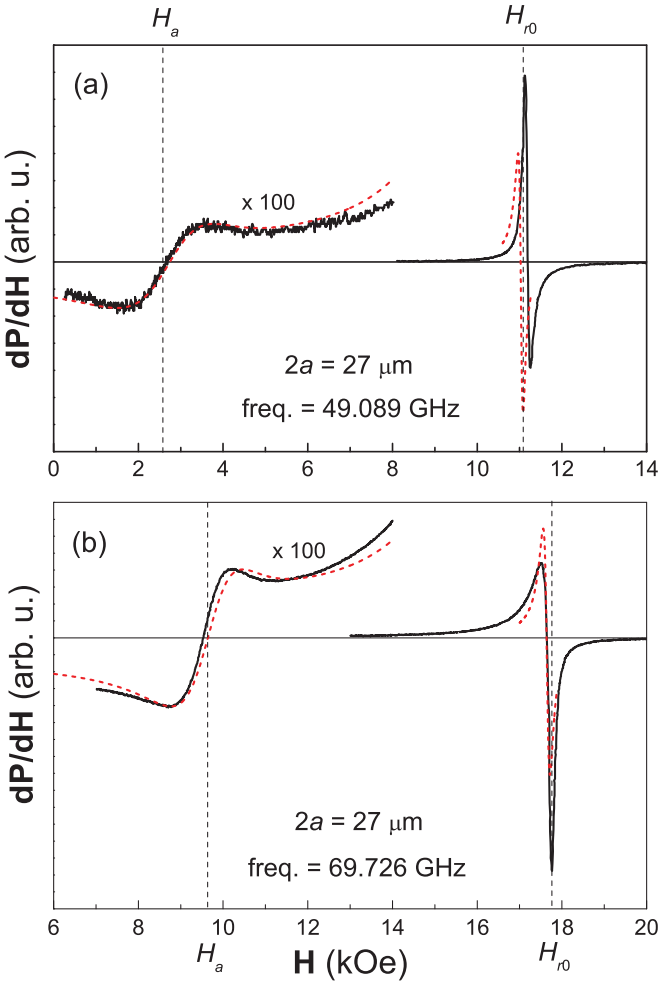


FIG. 10. (Color online) Resonance spectra for an amorphous FeSiBP microwire with metallic core diameter $2a = 27$ $\mu$m. (a) Microwave frequency of 49.1 GHz; (b) microwave frequency of 69.7 GHz. The full curves represent the experimental data, while the dashed curves are theoretically calculated.

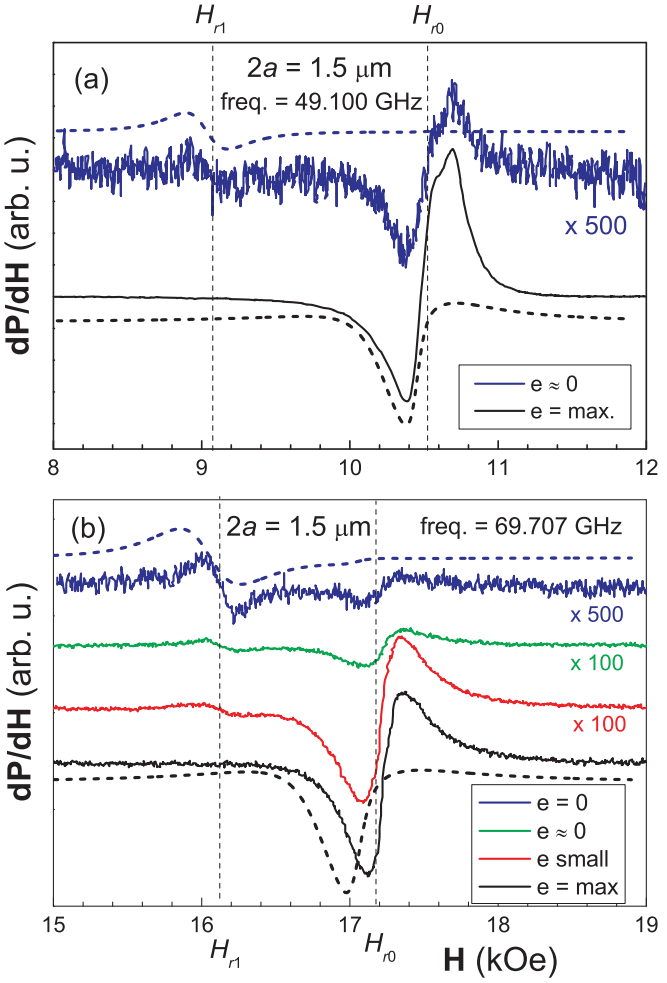


FIG. 11. (Color online) Resonance spectra for an amorphous FeSiBP microwire with metallic core diameter $2a = 1.5$ $\mu$m measured at different distances of the sample from the tuning plunger. (a) Microwave frequency of 49.1 GHz; (b) microwave frequency of 69.7 GHz. The full curves represent experimental data. The dashed curves depict the theoretically calculated $dP_1/dH$ and $dP_0/dH$, respectively.

The FMR spectra of the thin sample ($2a = 1.5$ $\mu$m) are shown by full curves in Fig. 11. When the sample is placed in the maximum of electric field (lower curve), a strong $n = 0$ resonance is observed. FMAR cannot be seen now because the wire radius $a$ is much smaller than the penetration depth of the electromagnetic wave, $U$, at antiresonance, as explained in Sec. V. When the sample position approaches the node of the electric field (upper curves), the intensity of the circular resonance mode sharply decreases and the dipolar mode ($n = 1$) becomes visible. The maximum intensity of this mode is about three orders of magnitude smaller than the intensity of circular mode in the "Rodbell position." Additionally, the field derivative of the two resonance curves shows the opposite sequence of minima and maxima, which means that the first represents a peak and the second a dip on the absorption curve $P(H)$. This result is in agreement with the observation of Lofland *et al.*[8] The resonance fields $H_{r0}$ and $H_{r1}$, calculated according to Eqs. (27) and (28), are represented by the vertical dashed lines. In order to properly fit the measured fields with the same parameters $g$ and $M_s$ an easy-wire-axis anisotropy with an anisotropy field $H_K = 0.6$ kOe is introduced. This anisotropy is ascribed to a strong internal strain due to the thick glass coat. The theoretically calculated curves $d\,\mathrm{Re}(\eta_0)/dH$ and $dP_1/dH$ are shown by the dashed curves. Once more, the experimental data agree qualitatively well with the theoretical predictions.

## VIII. CONCLUDING REMARKS

The correct interpretation of microwave absorption experiments in thin ferromagnetic wires requires a number of parameters to be considered carefully: the wire radius, the symmetry of microwave magnetic field at the sample surface, and the skin depth (both magnetic and nonmagnetic). It has been theoretically shown and experimentally verified that in thin metallic wires various resonance modes can be excited. The intensity and resonance fields of the individual modes depend on the wire diameter and the particular experimental arrangement. Mainly modes with the lowest azimuthal mode numbers ($n = 0, 1$) are effective in standard FMR experiments.

The circumferential (or metallic) mode, $n=0$, is strongly excited by the electric component of microwave field parallel to the wire axis. The much weaker dipolar (or insulator) mode, $n=1$, is excited by the magnetic component of the microwave field. For bulk wires (diameters larger than the nonmagnetic skin depth) these two modes practically coincide and satisfy the Kittel's resonance condition for a tangentially magnetized thin film. This is why in the vast majority of FMR experiments on wires only this resonance has been reported. When the wire diameter goes down to the nonmagnetic skin depth, the dipolar mode, $n=1$, separates from the circumferential mode. For small wire diameter the resonance condition of the $n=1$ mode approaches the Kittel's resonance condition of an axially magnetized long cylinder. The dipolar mode can be experimentally observed if the prevailing $n=0$ mode is eliminated by means of a proper experimental arrangement. It has been theoretically predicted that for wires with nano-sized diameters the dipolar mode becomes dominant.

The theoretical model, presented, also describes the existence of spin wave modes with various symmetries in wires of nanometric dimensions. The equations shown here can be used for numerical simulations in order to help understanding the influence of various parameters, such as the exchange stiffness or the surface anisotropy, on the resonance curves of microwires and nanowires.

## ACKNOWLEDGMENTS

This work was done in the frame of common project ASCR–CSIC "Magnetic properties of micro- and nano-magnetic heterostructures at RF and microwave frequencies" and was partly supported by the Grant Agency of the Czech Republic (Grant No. 102/08/0743), the Academy of Sciences of the Czech Republic (Grant No. AVOZ 10100520), and the Spanish Ministry of Science and Innovation (Project No. MAT2007-65420-C02-01). G.I. acknowledges the Spanish MICINN FPU fellowship program.

*Corresponding author: kraus@fzu.cz

[1] O. Reynet, A. -L. Adenot, S. Deprot, O. Acher, and M. Latrach, Phys. Rev. B **66**, 094412 (2002).
[2] D. P. Makhnovskiy and L. V. Panina, J. Appl. Phys. **93**, 4120 (2003).
[3] L. V. Panina, S. I. Sandacci, and D. P. Makhnovskiy, J. Appl. Phys. **97**, 013701 (2005).
[4] L. V. Panina, Phys. Status Solidi A **206**, 656 (2009).
[5] M. Darques, J. Spiegel, J. De la Torre Medina, I. Huynen, and L. Piraux, J. Magn. Magn. Mater. **321**, 2055 (2009).
[6] L.-P. Carignan, V. Boucher, T. Kodera, C. Caloz, A. Yelon, and D. Ménard, Appl. Phys. Lett. **95**, 062504 (2009).
[7] J. Carbonell, H. García-Miquel, and J. Sánchez-Dehesa, Phys. Rev. B **81**, 024401 (2010).
[8] S. E. Lofland, H. García-Miquel, M. Vázquez, and S. M. Bhagat, J. Appl. Phys. **92**, 2058 (2002).
[9] C. Kittel, Phys. Rev. **73**, 155 (1948).
[10] C. Kittel and C. Herring, Phys. Rev. **77**, 725 (1950).
[11] W. S. Ament and G. T. Rado, Phys. Rev. **97**, 1558 (1955).
[12] J. R. MacDonald, Phys. Rev. **103**, 280 (1956).
[13] Z. Frait and H. MacFaden, Phys. Rev. **139**, A 1173 (1965).
[14] Z. Frait and D. Fraitová, in *Modern Problems of Physics, Spin Waves and Magnetic Excitations*, edited by A. S. Borovik-Romanov and R. Sinha (Elsevier, Amsterdam, 1988), Part 2, p. 1.
[15] Z. Frait and D. Fraitová, in *Frontiers in Magnetism of Reduced Dimension Systems* (NATO ASI, Series 3, Vol. 49), edited by P. Wigen, V. Bar'yakhtar, and N. Lesnik (Kluver Academic, Dordrecht, 1998), p. 121.
[16] D. S. Rodbell, J. Appl. Phys. **30**, S 187 (1959).
[17] B. Heinrich, Czech. J. Phys. B **17**, 142 (1967).
[18] L. Kraus, Czech. J. Phys. B **32**, 1264 (1982).
[19] D. Ménard, M. Britel, P. Ciureanu, and A. Yelon, J. Appl. Phys. **84**, 2805 (1998).
[20] R. Arias and D. L. Mills, Phys. Rev. B **63,** 134439 (2001).
[21] D. Ménard and A. Yelon, J. Appl. Phys. **88**, 379 (2000).
[22] L. G. C. Melo, D. Ménard, P. Ciureanu, and A. Yelon, J. Appl. Phys. **92**, 7272 (2002).
[23] V. Boucher and D. Ménard, Phys. Rev. B **81**, 174404 (2010).
[24] G. T. Rado and J. R. Weertman, J. Phys. Chem. Solids **11**, 315 (1959).
[25] M. Knobel, M. Vázquez, and L. Kraus, in *Handbook of Magnetic Materials*, edited by K. H. J. Buschow, Vol. 15 (North-Holland, Amsterdam, 2003), p. 497.
[26] A. G. Gurevich and G. A. Melkov, *Magnetization oscillations and waves* (CRC, Boca Raton, FL, 1996).
[27] Y. J. Liu and R. C. Barker, AIP Conf. Proc. **24**, 505 (1974).
[28] C. A. Patton, Czech. J. Phys. B **26**, 925 (1976).
[29] The fourth "nonresonant" electromagnetic wave $E$ (or $AE$), which corresponds to the nonmagnetic skin effect for $\mathbf{h}$ parallel to $\mathbf{M}_0$, is not excited in the usual FMR experiments and is therefore neglected.
[30] S. N. Samaddar, Appl. Sci. Res., Sect. B **10**, 385 (1963).
[31] N. Bloembergen, J Appl. Phys. **23**, 1383 (1952).
[32] Equation (20) was originally derived for a planar surface in Cartesian coordinates. We have proved that it is also valid for a cylindrical surface in cylindrical coordinates.
[33] L. Kraus and M. Jirsa, J. Magn. Magn. Mater. **44**, 292 (1984).
[34] M. H. Johnson and G. T. Rado, Phys. Rev. **75**, 841 (1949).
[35] D. Ménard, M. R. Britel, P. Ciureanu, A. Yelon, V. P. Paramonov, A. S. Antonov, P. Rudkowski, and J. O. Strom-Olsen, J. Appl. Phys. **81**, 4032 (1997).
[36] L. Brunetti, P. Tiberto, and F. Vinai, Sens. Actuators, A **67**, 84 (1998).
[37] L. Kraus, M. Vázquez, G. Infante, G. Badini-Confalonieri, and J. Torrejón, Appl. Phys. Lett. **94**, 062505 (2009).
[38] V. Raposo, G. Infante, M. Zazo, and J. Iniguez, *Measuring Magnetoimpedance in Multilayer Amorphous Microwires*, in Proceedings of International Conference on Magnetic Measurements, Prague, 2010 (unpublished).
[39] H. García-Miquel, J. M. García, J. M. García-Beneytez, and M. Vázquez, J. Magn. Magn. Mater. **231**, 38 (2001).
[40] D. S. Rodbell, J. Appl. Phys. **30**, 1845 (1959).
[41] L. Kraus and A. N. Anisimov, J. Magn. Magn. Mater. **58**, 107 (1986).
[42] G. F. Taylor, Phys. Rev. **23**, 655 (1924).
[43] A. V. Ulitovsky, I. M. Maianski, and A. I. Avramenco, *Method of continuous casting of glass coated microwire*, USSR Patent No. 128427 (1960).